Effects of Long-Term *In vivo* Stimulation on the Electrochemical Properties of a Porous Stimulation Electrode for a Suprachoroidal–Transretinal Stimulation (STS) Retinal Prosthesis

Shuhei Nomura,[1–3] Hiroyuki Tashiro,[2,3*] Yasuo Terasawa,[2,4,5] Yukari Nakano,[5] Makito Haruta,[4,6] Kiyotaka Sasagawa,[3] Hironari Takehara,[3] Takeshi Morimoto,[7] Takashi Fujikado,[8] and Jun Ohta[3,4]

[1]Department of Medical Technology, Faculty of Fukuoka Medical Technology, Teikyo University, 6-22 Misakimachi, Omuta, Fukuoka 836-8505, Japan
[2]Department of Health Sciences, Faculty of Medical Sciences, Kyushu University, 3-1-1 Maidashi, Higashi-ku, Fukuoka 812-8582, Japan
[3]Division of Materials Science, Graduate School of Science and Technology, Nara Institute of Science and Technology, 8916-5 Takayama-cho, Ikoma, Nara 630-0192, Japan
[4]Research Laboratory on Next Generation Biomedical Engineering, Institute for Research Initiatives, Nara Institute of Science and Technology, 8916-5 Takayama-cho, Ikoma, Nara 630-0192, Japan
[5]Artificial Vision Institute, Research and Development Division, Nidek Co., Ltd., 13-2 Hama-cho, Gamagori, Aichi 443-0036, Japan
[6]Department of Opto-Electronic System Engineering, Faculty of Science and Engineering, Chitose Institute of Science and Technology, 758-65 Bibi, Chitose, Hokkaido 066-8655, Japan
[7]Department of Advanced Visual Neuroscience, Graduate School of Medicine, Osaka University, 2-2 Yamadaoka, Suita, Osaka 565-0871, Japan
[8]Graduate School of Frontier Biosciences, Osaka University, 1-3 Yamadaoka, Suita, Osaka 565-0871, Japan

A high-performance porous stimulation electrode [femtosecond laser-induced porosity (FLiP) electrode] was designed for the safe and effective delivery of high stimulation currents. Herein, we evaluated the electrochemical properties of the FLiP electrode interface under prolonged *in vivo* stimulation. The FLiP electrodes were surgically implanted in rabbits and subjected to stimulation currents over a six-month period. The impedance of these electrodes was examined through equivalent circuit analysis, specifically employing the Randles circuit model. Comparative analysis with the results of previous *in vitro*/*in vivo* studies was conducted. Electrical stimulation served to purify the electrode interface, enhancing mass diffusion and promoting charge-transfer reactions at the electrode interface. As a result, the electric double-layer capacitance (C_{dl}) could be enhanced by adjusting the ionic concentration at the electrode. The high charge injection capacity of the FLiP electrode is facilitated by not only capacitive currents resulting from C_{dl} but also pseudocapacitive currents stemming from the reversible redox reaction of H_2 molecules. Our findings suggest that the initial evaluation outcomes can

extrapolate the electrode properties during long-term stimulation, and the combined method of electrochemical impedance spectroscopy and equivalent circuit analysis clarifies intricate *in vivo* interactions, allowing accurate analysis of the properties of implantable electrodes over extended periods.

1. Introduction

Retinal prostheses restore a lost visual function by stimulating the partially dysfunctional retina[1–3] through the application of safe currents via implanted electrodes and mainly target retinitis pigmentosa and age-related macular degeneration. Although these diseases cause the degeneration of retinal photoreceptor cells (and hence, blindness), they do not induce the complete loss of retinal functions, i.e., the transmission of visual information to the brain is not fully terminated.[4]

Depending on the location of the implanted electrodes, [5] retinal prostheses are classified into those using epiretinal,[6] subretinal,[3] or suprachoroidal–transretinal stimulation (STS).[7,8] To date, the STS-type retinal prostheses have been evaluated in clinical trials,[9,10] and other prostheses of this type are currently under development.[11,12] Compared with prostheses relying on other stimulation techniques, the STS-type retinal prostheses feature the advantages of less invasive surgery and more stable electrode fixation, as the corresponding stimulation electrode array is implanted into a scleral pocket and electrically stimulates the retina through the choroid.[10] However, the large separation between the stimulation electrode and the retina necessitates the application of high-stimulation currents to induce a light sensation (phosphene). Consequently, a high-performance porous stimulation electrode, namely, a femtosecond laser-induced porosity (FLiP) electrode, was developed to safely and effectively apply high stimulation current for long periods.[13]

The FLiP electrode exhibits a three-dimensional porosity and has a large real surface area relative to its geometric surface area, thus featuring a high charge injection capacity (CIC, the amount of charge per unit area that can be injected at electrode potentials within the water potential window). However, the electrochemical behavior at the interface of this porous stimulation electrode *in vivo* is complex and still not well understood.

A previous *in vivo* study showed that the impedance of the FLiP electrode decreases immediately after stimulation;[14] however, the underlying mechanism is still unclear. Such complex phenomena influenced by multiple factors can be efficiently probed using equivalent circuit analysis (ECA).[15,16] A comparison between the ECA results and other *in vitro/in vivo* experimental results can facilitate the design of implantable stimulation electrodes, which can improve their safety, reduce the need for animal testing, and accelerate the development of retinal prostheses.

In this study, electrochemical impedance spectroscopy (EIS)-ECA was employed to evaluate the impedance of an implanted FLiP electrode during a six-month chronic *in vivo* stimulation. The relationships between the equivalent circuit elements were assessed and the resulting changes in the electrode electrochemical properties were then elucidated.

2. Methods

2.1 Electrical stimulation

Bullet-shaped Pt stimulation electrodes (diameter = 500 μm, height = 300 μm, geometric surface area = 0.0043 cm^2) were subjected to a femtosecond laser processing that created laser holes (hole diameter = 10 μm, hole depth = ~100 μm) and resulted in a microstructured surface both on the inside and outside the laser holes on the electrode surface (Fig. 1). Subsequently, a platinum wire was wired to each porous electrode (FLiP electrode) prior to placing them on a parylene C substrate (thickness = 30 μm).[13] The stimulation electrode array was implanted into the scleral pockets of Japanese white rabbits (N = 5) [Fig. 2(a)].[14,17] The return electrode was fabricated from a Pt bar (length = 3 mm, diameter = 500 μm) and implanted into the vitreous cavity via the pars plana. To evaluate the effect of stimulation on the electrode characteristics, a stimulation current was applied between one of the two FLiP electrodes (active electrode) and the return electrode, while no current was applied to the other electrode (inactive electrode). The two FLiP electrodes were surrounded by dummy electrodes fabricated from parylene C to reduce the mechanical stress between the electrode and the retina/choroid. The electrical stimulation (Table 1) was initiated two weeks after implantation and continued for six months.[14]

This animal study was approved by the institutional animal care and use committee of Nidek Co., Ltd. All *in vivo* experiments were conducted in accordance with the Association for Research in Vision and Ophthalmology (ARVO) Statement for the Use of Animals in Ophthalmic and Visual Research.[18]
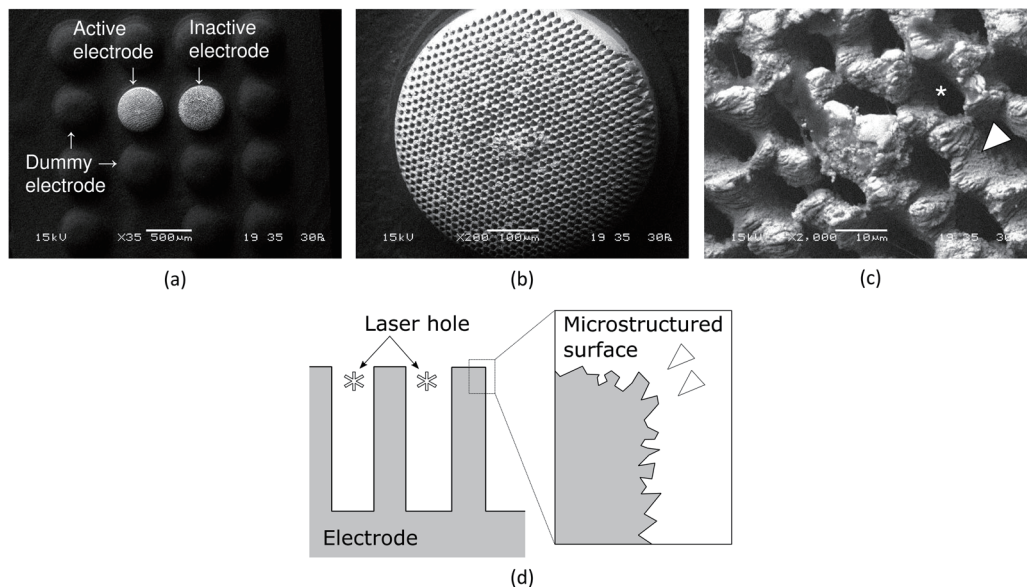

Fig. 1.   SEM images[15] of (a) electrode array with two porous electrodes and (b and c) active electrode surface. (d) Electrode surface structure with holes created by the laser porosity process [asterisk in (c)] and the microstructured surface on the inside and outside of the laser holes [arrow in (c)]. Reproduced with modification with permission from John Wiley and Sons, Inc.
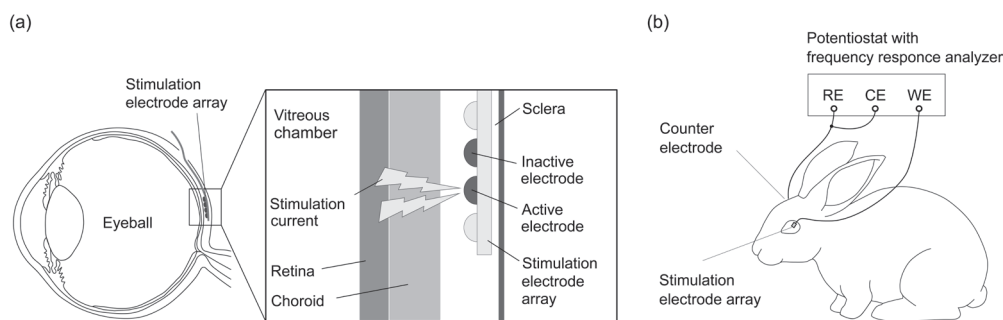
Fig. 2.   Schematic illustrations of the (a) installation of suprachoroidal–transretinal stimulation electrode array[15] (the array was inserted into scleral pockets and the retina was electrically stimulated through the choroid. Reproduced with modification with permission from John Wiley & Sons, Inc.) and (b) setup for the electrode-impedance measurement.[14] Reproduced with modification with permission from MYU K. K.

Table 1
Parameters of suprachoroidal–transretinal stimulation.

Pulse polarity	Cathodic-first biphasic
Pulse amplitude	1.5 mA
Pulse duration	500 μs
Interpulse duration	50 μs
Repetition frequency	50 Hz
Stimulation time	8 h per day

2.2   EIS

The electrochemical impedance between the stimulation and the counter electrodes during the stimulation period was measured in a two-electrode configuration [Fig. 2(b)]. Specifically, a 20 mV_{rms} sine wave in the frequency range of 10 Hz to 100 kHz was applied using a potentiostat equipped with a frequency response analyzer (Autolab PGSTAT 12, Metrohm, Utrecht, Netherlands).[14] The counter electrode, a Pt wire with a diameter of 0.5 mm and a surface area of >1 cm^2, was subcutaneously implanted into the temporal region on the opposite side of the stimulated eye. The influence of the counter-electrode impedance was ignored, as this electrode had a sufficiently large surface area and was located far from the stimulation electrode, i.e., at a distance significantly exceeding the dimensions of the latter.[14]

2.3   ECA

The EIS data acquired during the six-month stimulation were subjected to ECA (NOVA electrochemical analysis software, Metrohm, Utrecht, the Netherlands). The equivalent circuit model was based on a Randles circuit model reflecting the characteristics of the FLiP electrode interface and included the following four elements: solution resistance (R_{sol}), diffusion resistance

(Warburg impedance, Z_W), charge-transfer resistance (R_{ct}), and electric double-layer capacitance (C_{dl}) (Fig. 3).[15,16] R_{sol} reflects the resistance of the bulk solution, R_{ct} reflects the difficulty of charge-transfer reactions such as oxidation and reduction at the electrode interface, C_{dl} reflects the capacitance of the electric double layer formed at the electrode–electrolyte interface, and Z_W reflects the resistance of ion diffusion at low frequencies [Eqs. (1) and (2)] (Fig. 4).

$$Z_W = \frac{\sigma}{\sqrt{\omega}}(1-j),$$ (1)

$$\sigma = \frac{RT}{\sqrt{2}\, n^2 F^2 A_r} \left(\frac{1}{\sqrt{D_O}\, C_O} + \frac{1}{\sqrt{D_R}\, C_R} \right),$$ (2)

where j is an imaginary unit, ω is the angular frequency, σ is the Warburg coefficient, R is the gas constant, T is the absolute temperature, n is the valence number, F is the Faraday constant, A_r
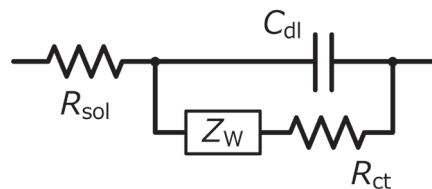

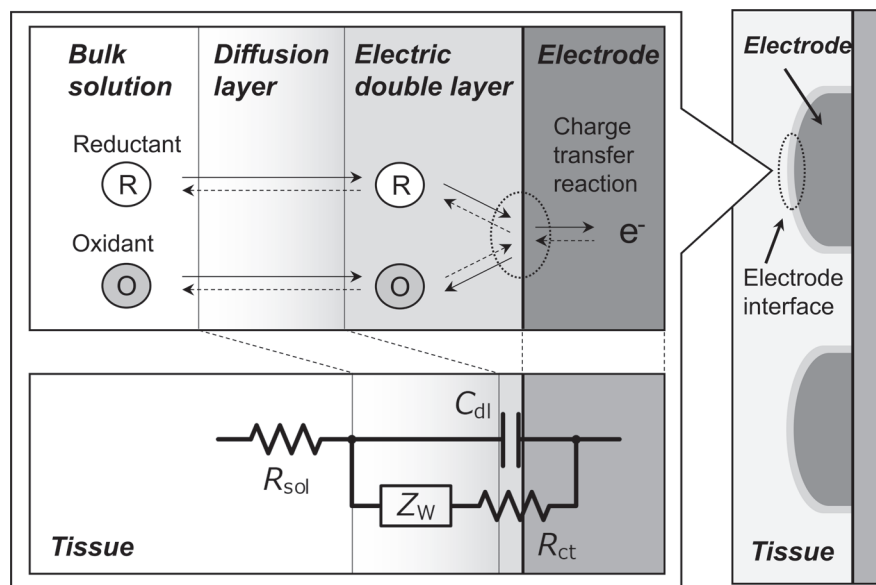Fig. 3.   Randles circuit model simulating the porous stimulation electrode.

Fig. 4.   Correspondence between an electrochemical reaction process and the equivalent circuit elements shown in Fig. 3. The electric double layer and diffusion layer are formed at the electrode–bulk solution interface. The reactive species in the tissue solution are oxidized or reduced by charge-transfer reactions at the electrode interface, with the reactants and products transported to/from the electrode surface and the bulk solution through the diffusion layer.[15] Reproduced with modification with permission from John Wiley and Sons, Inc.

is the electrode area, D_O is the oxidant diffusion coefficient, D_R is the reductant diffusion coefficient, C_O is the oxidant concentration, and C_R is the reductant concentration.

2.4 CIC

Theoretically, CIC is defined as the maximum charge density attainable within the water potential window (−0.6 to +0.8 V vs Ag/AgCl for Pt electrodes[19,20]) during charge injection [Fig. 5(a)]. However, even with a stimulation current in this range, platinum elution (an irreversible reaction) occurs in both the simulated biological solution[21–23] and living tissue.[24] In addition, various chemical species present in the living body but not contained in the simulated biological solution cause redox reactions within the potential window of water, thus affecting the CIC value.[25] Therefore, strictly speaking, water electrolysis occurs even within the water potential window (−0.6 V to +0.8 V vs Ag/AgCl, Pt electrode). However, due to the buffering functions of the living body, the living tissue is not immediately damaged.[26] The determination of CIC within this potential window is a conservative estimation for safety. Therefore, although this potential range is widely used as the threshold for a safe assessment, it does not mean that irreversible reactions do not occur within this range. The R_{ct} values obtained from the EIS-ECA, which applies a minute measurement potential (20 mV$_{rms}$), reflect the difficulty of redox reactions to occur within the water potential window. If the electric double-layer formation at the electrode surface is ideal, then R_{ct} should be infinite because, in the simulations of this study, the diffusion resistance Z_w was separated from R_{ct}.

For the *in vivo* CIC measurements, a cathodic-first biphasic pulse with a duration of 0.5 ms and a repetition frequency of 30 Hz was applied between the stimulation (working) and intravitreous Pt-bar (counter) electrodes [Fig. 5(b)]. A 50 µs open-circuit period was inserted as an interpulse gap between the first cathodal pulse and the second anodal pulse as well as after the second pulse. The electrode potential was recorded using a custom-built amplifier and oscilloscope (DL750, Yokogawa Meters & Instruments, Tokyo, Japan).[14] An Ag/AgCl reference
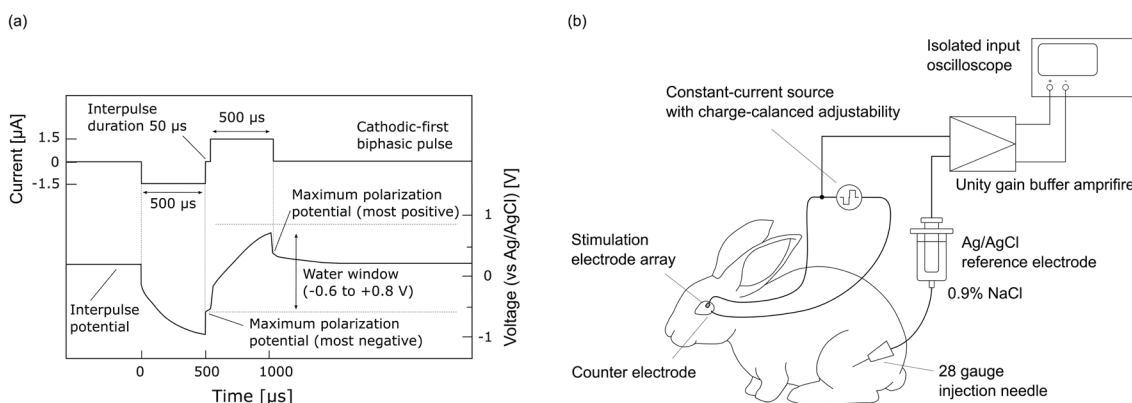

Fig. 5. Experimental illustration of the CIC measurement. (a) Response of the electrode potential to the stimulation current.[14] (b) Setup for the CIC measurement.[14] Reproduced with modification with permission from Myu K. K. Co., Ltd.

electrode (Ag/AgCl, International Chemistry Co., Ltd., Chiba, Japan) immersed into a salt bridge prepared in a tube filled with physiological saline was electrically connected to each rabbit. The electrode potential at the end of each pulse was defined as the polarization potential without the ohmic drop. The maximum current within the range where the polarization potential immediately after the first or second pulse was not outside the water potential window[14] was multiplied by the pulse duration to determine the amount of injected charge. CIC was sampled on a monthly basis as the ratio of the injected charge to the geometric surface area of the FLiP electrode (0.0043 cm^2).

2.5 Evaluation of stimulation electrode morphology

The surface of the stimulation electrode before and after implantation was observed using SEM (JSM-5600LV, Japan Electron Optics Laboratory, Tokyo, Japan). Prior to observation, the explanted electrodes were cleaned for >3 h at 50 °C in a 0.1% enzyme solution (Bioplase AL-15-FG, Nagase ChemteX, Osaka, Japan) to remove surface-adhered organic materials.[13]

2.6 Data analysis

For each equivalent circuit element, a two-way repeated measures analysis of variance (rANOVA) was performed to evaluate the effects of two nominal scale factors (*stimulation* and *period*) and their *interaction*. For the post-hoc testing, Tukey's HSD test was performed in both the active and inactive groups (significant difference: $p \leq 0.05$). The relationship among the equivalent circuit elements, experimentally determined electrode impedance, and CIC was investigated by correlation analysis. For the statistical analysis, each monthly value was calculated by averaging the daily measured values. The results of inaccurate measurements due to animal body movements or disconnection-related problems were excluded. Analysis was carried out using JMP Pro 16 software (SAS Institute Inc., Cary, NC, USA). The data are presented as means ± standard deviations (SDs).

3. Results

The electrode impedance was automatically measured at regular intervals. As a substantial amount of data was discarded because of animal body movements or wiring disconnection, one of the inactive electrodes (electrode No. 2) was excluded. Thereby, the sample sizes (N) for the active and inactive electrodes were 5 and 4, respectively.

3.1 R_{sol}

The results of the two-way rANOVA for R_{sol} showed significant differences in stimulation and period (Table 2). In the case of the active electrode, the first-month value (1.60 ± 0.23 kΩ) was lower than the prestimulation value (2.11 ± 0.18 kΩ) by 24% (0.51 kΩ) and did not change

Table 2
Results of two-way rANOVA (active electrode vs. inactive electrode). The effects of *stimulation*, *period*, and their *interaction* were evaluated for changes in each equivalent circuit element.

Equivalent circuit element	Factors					
	Stimulation		*Period*		*Interaction* of *stimulation* and *period*	
	F-value	*p*-value	*F*-value	*p*-value	*F*-value	*p*-value
R_{sol}	24.44	$\leq 0.01^{**}$	2.41	0.04^{*}	2.21	0.06^{NS}
R_{ct}	17.6	$\leq 0.01^{**}$	13.12	$\leq 0.01^{**}$	4.06	$\leq 0.01^{**}$
Z_W	4.24	0.08^{NS}	8.56	$\leq 0.01^{**}$	0.53	0.78^{NS}
C_{dl}	1.56	0.25^{NS}	1.68	0.15^{NS}	0.84	0.55^{NS}

NS: not significant ($p > 0.05$), *: significant ($p \leq 0.05$), **: significant ($p \leq 0.01$).

later on [Fig. 6(a)]. For the inactive electrode, no change in R_{sol} was observed over six months, i.e., the mean and variation range (2.03 ± 0.33 kΩ) did not change during stimulation [Fig. 6(b)].

3.2 R_{ct}

The results of the two-way rANOVA for R_{ct} showed significant differences in stimulation, period, and their interaction (Table 2). In the case of the active electrode, the first-month value (0.57 ± 0.22 kΩ) was lower than the prestimulation value (6.94 ± 3.09 kΩ) by 92% (6.37 kΩ) [Fig. 6(c)]. The variation range of R_{ct} (SD = 0.06–0.22 kΩ) after the first month was lower than that observed before stimulation (SD = 3.09 kΩ) and did not change at later times [Fig. 6(c)]. In the case of the inactive electrode, no change in R_{ct} was observed over time, i.e., the mean and variation range (4.22 ± 1.59 kΩ) did not change during stimulation [Fig. 6(d)].

3.3 Z_W

The results of the two-way rANOVA for Z_W showed significant differences in period (Table 2). In the case of the active electrode, the first-month value (28.4 ± 3.9 kΩ s$^{-0.5}$) was lower than the prestimulation value (256.2 ± 218.6 kΩ s$^{-0.5}$) by 89% (227.7 kΩ s$^{-0.5}$) [Fig. 6(e)]. The variation range (SD = 3.9–9.1 kΩ s$^{-0.5}$) after the first month was lower than that before stimulation (SD = 218.6 kΩ s$^{-0.5}$) and remained unchanged at later times [Fig. 6(e)]. In the case of the inactive electrode, a slight decrease was observed after one-month stimulation (317.8 ± 249.7 kΩ s$^{-0.5}$) [Fig. 6(f)].

3.4 C_{dl}

The results of the two-way rANOVA for C_{dl} showed no significant difference (Table 2). In the case of the active electrode, the first-month mean C_{dl} (21.1–27.2 nF) and its variation range (11.7–13.5 nF) exceeded the values observed before stimulation (14.2 ± 2.9 nF) by factors of 1.5–1.9 and 4.0–4.7, respectively [Fig. 6(g)]. In the case of the inactive electrode, C_{dl} did not change with time, and the corresponding variation range remained very close to that observed before stimulation (12.9 ± 4.8 nF) [Fig. 6(h)].
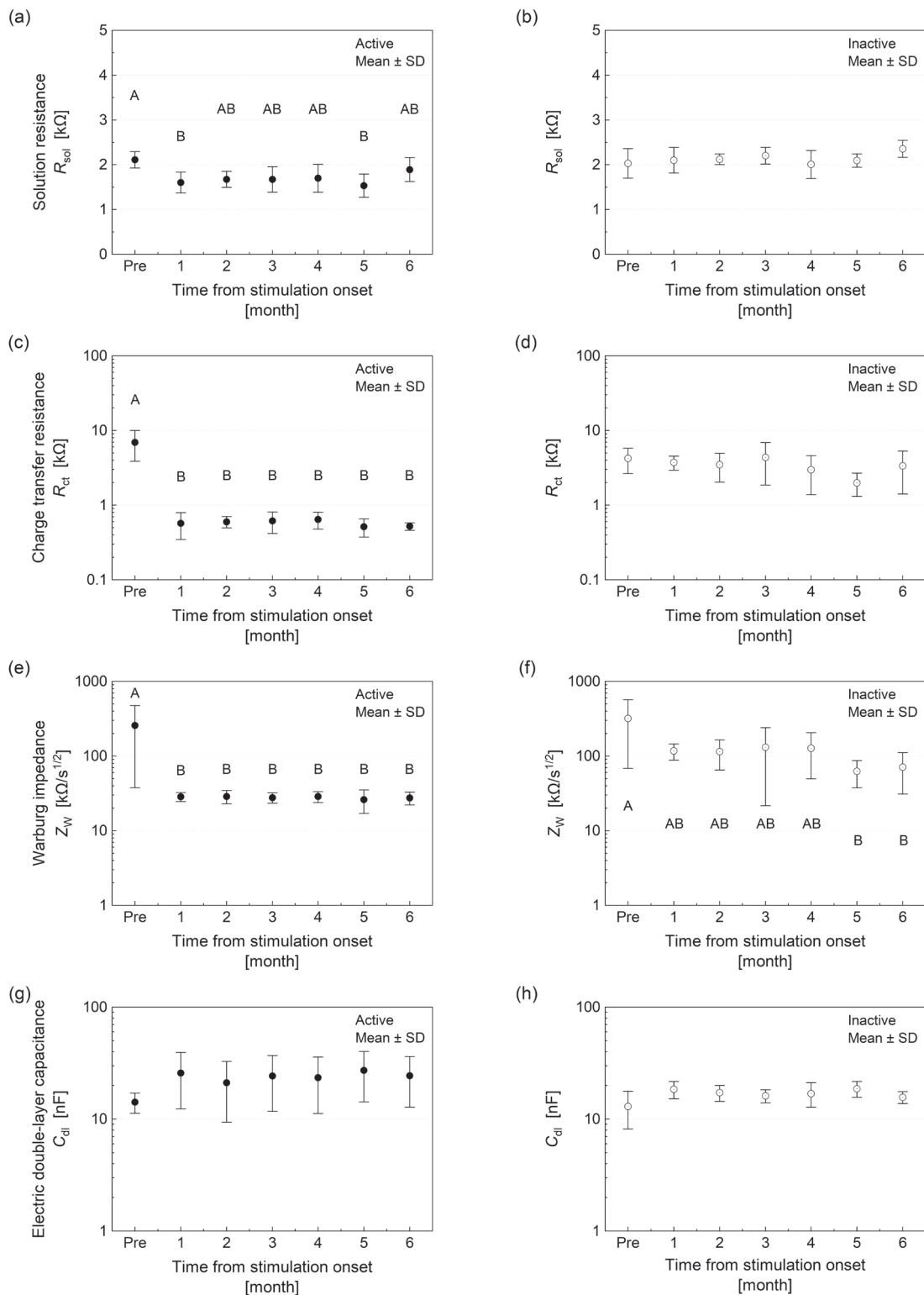
Fig. 6.   Effects of stimulation time on (a, b) R_{sol}, (c, d) R_{ct}, (e, f) Z_{W}, and (g, h) C_{dl} observed for (a, c, e, g) active and (b, d, f, h) inactive electrodes. Different letters (A and B) indicate significant differences according to Tukey's HSD test ($p \leq 0.05$). Groups indicated by the same letters or no letters are not significantly different from each other (Tukey's HSD test, $p > 0.05$).

3.5   SEM images of electrode surface

The SEM images of the preimplanted and extracted electrodes (Fig. 7) revealed the presence of surface-adhered proteins in the latter case [Figs. 7(b)] and the absence of damage due to electrode elution [Figs. 7(c)].

3.6   Correlations analysis

The correlation analysis was performed to analyze the correlations between the simulated values of the equivalent circuit elements (R_{sol}, R_{ct}, Z_W, and C_{dl}) and the experimentally measured active electrode impedance (Z) and CIC (Fig. 8).

R_{sol} was positively correlated with Z in the high-frequency range (0.1–10 kHz). Z_W and R_{ct} were positively correlated with Z in the low-frequency ranges of 0.01–0.1 and 0.1–1 kHz, respectively. C_{dl} was positively correlated with R_{sol} and negatively correlated with Z_W and CIC. CIC was negatively correlated with Z at 0.1 kHz ($Z_{0.1\ kHz}$).

4.   Discussion

4.1 R_{sol}

The fact that R_{sol} remained relatively stable over the stimulation period was ascribed to electrode encapsulation (foreign body reaction) and the desorption of adsorbed protein. In general, for electrodes implanted into a living body, R_{sol} increases because of their encapsulation by fibrotic tissue after protein absorption.[27] The adsorption of protein on the electrode surface increases R_{sol} and decreases C_{dl}.[28] Upon the application of a stimulation current, the adsorbed protein is desorbed, and the electrode surface is cleaned up.[29] Herein, R_{sol} decreased at the onset of stimulation and remained relatively stable during the six-month stimulation period
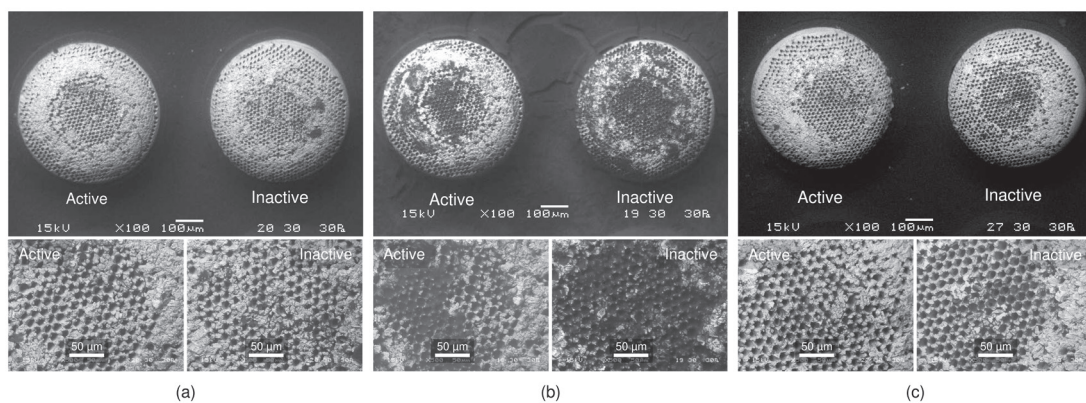

Fig. 7.   SEM images of (a) preimplanted and (b and c) extracted electrodes [(b) before and (c) after cleaning]. Magnified images of (left) active and (right) inactive electrodes. Biomolecules such as proteins adhered to the surface of the extracted electrode before washing (b). No significant electrode degradation such as elution was observed (c).
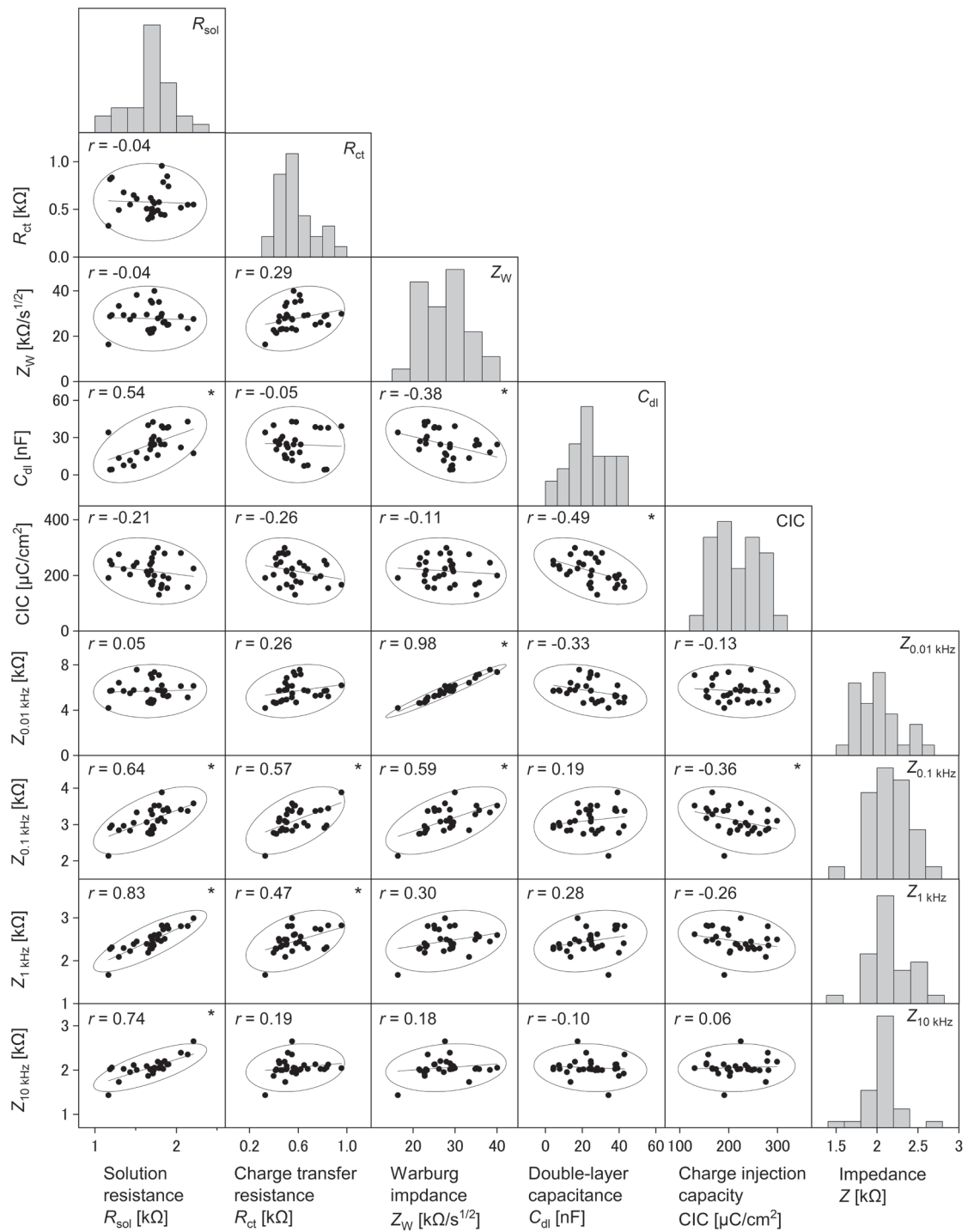
Fig. 8.　Results of the correlation analysis in active electrodes between each equivalent circuit element (R_{sol}, R_{ct}, Z_W, and C_{dl}) and the experimentally measured data (CIC and Z). Ellipses are drawn at the 95% confidence level, r: Pearson's correlation coefficient, p: p-value of test-for-no-correlation, *: significant ($p \leq 0.05$).

[Figs. 6(a) and 6(b)]. The two-way rANOVA revealed that stimulation and period significantly influenced R_{sol} (Table 2), thus reflecting the effects of encapsulation progression and protein desorption.

R_{sol} is the major contributor to the ohmic drop (iR-drop) (= R_{sol} × stimulation current) in microelectrodes implanted into a living body. The power supply voltage must be sufficiently high to preserve a constant current output. The ohmic drop and polarization potential determine the current load for its application in the living body [Fig. 5(a)]. These values are useful in estimating the driving voltage of the stimulator to apply constant-current pulses to the living body when designing an artificial retinal device. Generally, DC-blocking capacitors are inserted between the electric circuit and either or both the stimulation and counter electrodes. In addition to the ohmic drop, the capacitor charge-up voltage must be considered as the current load.

In this study, the maximum estimated value of R_{sol} was ~2.52 kΩ. An iR drop of ~3 V is estimated when a stimulation current of 1 mA is applied to this R_{sol}. Since the maximum value of the polarization potential of the electrode used in this experiment is reported to be approximately −1.14 V when a current of 1.2 mA is applied,[14] estimating a polarization voltage of ~2 V is sufficient. The maximum charge-up voltage for the DC-blocking capacitor due to the application of the stimulation current pulse can be calculated by multiplying the current amplitude by the pulse duration and dividing this factor by the capacitance of the DC-blocking capacitor. For example, a 1 µF DC-blocking capacitor and a 1 mA–500 µs stimulation current pulse results in a capacitor charging voltage of 0.5 V. Even if the duration is extended to 1 ms, the charge voltage will be ~1 V. In such active implantable devices, a current mirror circuit with a cascode configuration is generally used for the constant-current generator circuit.[30,31] For a current-mirror current source to operate properly as a constant-current source, a certain voltage must be applied to the drain terminal for the FETs in the circuit to operate in the saturation mode. This voltage depends on the process by which the IC was manufactured. Since our device uses a high-voltage process to output stimulation currents of the order of mA, a voltage of approximately 1.5 V must be applied to the drain terminal of the FET.

Considering the design margin for these total values, a power supply voltage of ~10 V is required. This value depends on the stimulation current required to evoke a neural excitation and the IC manufacturing process. Thus, the equivalent circuit analysis reported in this study helps estimate the load voltage required to flow a constant stimulation current through the stimulation electrode to the electronic circuit.

The stability of R_{sol} during the six-month stimulation period [Figs. 6(a) and 6(b)] is useful for the design of power systems providing a sufficient stimulation current. In the case of STS, the effect of the ohmic drop is relatively large because of the high stimulation current, whereas for other types of retinal stimulations, the effect of the polarization potential is large because of the low stimulation current. The magnitude of the ohmic drop and the polarization potential effects depend on the electrode geometry (size and roughness)[28] and stimulation current parameters (amplitude and duration). If the polarization potential is much more significant than the ohmic drop (i.e., the stimulation current is tiny), then the polarization potential should be the primary consideration when designing the voltage source.

4.2 Z_W and R_{ct}

Protein adsorbed on the electrode surface reduces its effective area and affects charge transfer and mass diffusion.[25] Z_W reflects the difficulty of ion diffusion on the electrode surface in the low frequency range, whereas R_{ct} reflects the difficulty of electrochemical (redox) reactions involving electron transfer across the electrode–electrolyte interface.[32] R_{ct} increases upon protein adsorption, as the protein adsorbed on the implanted electrode inhibits carrier transfer.[28] Upon the application of a stimulation current, the adsorbed protein is desorbed, and the electrode surface is cleaned up, which facilitates mass diffusion and charge-transfer reactions.[25] Herein, Z_W and R_{ct} decreased immediately after the stimulation onset and subsequently remained stable [Figs. 6(c)–6(f), Table 2], which suggests that the stimulation current induced the desorption of the adsorbed protein from the active electrode surface. The amount of protein adhering to the surface of the extracted active electrode was lower than that observed for the inactive electrode [Fig. 7(b)]. It was thus concluded that the large variations in the R_{ct} and Z_W of the inactive electrodes are due to the uneven amounts of protein adhered thereon.[25]

Z_W did not directly affect the performance of the stimulation electrode for retinal prostheses because the frequency component of the stimulation current was significantly high relative to the diffusion velocity. However, Z_W was needed to fit the data to the equivalent circuit model and estimate other circuit elements.[16]

4.3 C_{dl}

The increase in C_{dl} after stimulation reflects the improved formation of the electric double layer due to the clean-up of the electrode surface by the stimulation current. The C_{dl} of the stimulation electrode represents its ability to induce a charge flow in the electrolyte without an electron transfer (capacitive current),[32] which contributes to CIC.[19] Therefore, high-C_{dl} electrodes can safely inject large electrical charges.[19] C_{dl} decreases upon the adsorption of protein on the electrode surface.[28] Despite the absence of a statistically significant difference due to the large variation, the mean value and variation range of the active-electrode C_{dl} increased immediately after the stimulation onset and remained stable thereafter [Figs. 6(g) and 6(h), Table 2]. These results indicate that the electrode surface was cleaned up because of the desorption of adsorbed protein by the stimulation current. The change in ion concentration contributes to the electric double layer formation. According to the Gouy–Chapman–Stern model, the electric double layer at the electrode interface is represented by the series connection of the electric double layer in the Helmholtz layer (capacity = C_H) and the outer diffusion layer (capacity = C_{diff}) [Eq. (3)]. The diffusion layer [capacity = C_{diff}; Eq. (4)] is described by the Gouy–Chapman theory, which shows that the concentration of ions causes the increase in C_{diff}.[33]

$$\frac{1}{C_{dl}} = \frac{1}{C_H} + \frac{1}{C_{diff}},$$

(3)

$$C_{\text{diff}} = \sqrt{\frac{2\varepsilon z^2 F^2 C_x^0}{RT}} \cosh\left[\frac{zF\psi_{\text{d}}}{2RT}\right], \tag{4}$$

where ε is the dielectric constant of the solvent, z is the ion valence number, F is the Faraday constant, C_x^0 is the total ion concentration in the bulk solution, R is the gas constant, T is the absolute temperature, and ψ_{d} is the electrostatic potential.

For the active electrode, the large variation in C_{dl} during stimulation was due to the electrolysis of water caused by the stimulation current. When a stimulation current of 1.2 mA is applied to the FLiP electrode implanted into a living body, the electrode potential on the cathode side extends beyond the water potential window and thus induces water electrolysis (water reduction: $2H_2O + 2e^- \rightarrow H_2\uparrow + 2OH^-$).[14] Therefore, the stimulation current of 1.5 mA applied herein (current density = 175 μC cm^{-2}) caused water electrolysis at the active electrode. On the active electrode, the oxidation film formation and water electrolysis caused changes in the ion concentration and H_2 molecule generation on the electrode interface, which resulted in an increase in C_{dl} during stimulation.[33] Therefore, the change in ion concentration around the active electrode surface caused an increase in C_{dl}.

4.4　Correlation between C_{dl} and CIC

Because C_{dl} contributes to the reversible capacitive current, a decrease in C_{dl} leads to a lower CIC, which increases the risk of harmful irreversible reactions. Generally, C_{dl} should be positively correlated with CIC. However, such correlation was not observed for the FLiP electrode (Fig. 8) because of the contribution of pseudocapacitive currents (caused by the reversible redox reaction of the H_2 molecules) to the CIC. The cyclic voltammogram of the FLiP electrode recorded between -0.85 and 0.3 V vs Ag/AgCl in phosphate-buffered saline featured a peak around 0 V that was not observed for the smooth Pt electrodes and was presumably due to the redox reaction of the H_2 molecules.[34] Generally, for the smooth planar Pt electrode, the generation of the H_2 molecules via water electrolysis is an irreversible reaction because the generated molecules diffuse and disappear from the electrode interface (the reaction field), causing an undesirable Faraday current.[19]

In contrast, in the case of the FLiP electrode, the H_2 molecules generated by water electrolysis were trapped in the surface pores, causing a reversible redox reaction.[13] Such reactions caused by reactive species remaining in the reaction field induce a pseudocapacitive current that contributes to an increase in CIC.[19] The unique feature of the FliP electrode is that the contributions of the capacitive current induced by C_{dl} and the pseudocapacitive current induced by the reversible redox reaction of the H_2 molecules improve the CIC.

4.5　Correlation between Z and CIC

Monitoring CIC as a safety indicator of stimulation performance is challenging because measuring CIC in clinical settings is difficult. Therefore, Z is a promising indicator for the

periodic monitoring of the device status, as it is easily obtained by measuring the voltage drop when a stimulation current is applied to the electrode. In active implantable devices, such as cochlear implants and retinal prostheses, Z [generally, Z at 1 kHz ($Z_{1\ kHz}$)[35]] is periodically measured by back-telemetry to monitor the device integrity (e.g., power status and wire breakage) during clinical applications.[36–38]

In this study, a significant correlation between CIC and $Z_{0.1\ kHz}$ was observed (Fig. 8), because of the large influence of R_{ct} (which reflects the reversible redox reaction of the H_2 molecules) and Z_W in the low-frequency range around 0.1 kHz. However, this correlation was weak ($r = -0.36$) because of several factors affecting the FLiP electrode, including the (1) ohmic drop during stimulation, (2) *in vivo* environmental changes around the implanted electrode, and (3) individual electrode differences due to the manufacturing process. Each factor will be discussed individually. First, in the case of STS using the microsized FLiP electrode, R_{sol} is the major component of Z because the ohmic drop accounts for a larger proportion of the electrode potential than the polarization potential. Therefore, compared with those of R_{sol}, the effects of CIC, C_{dl}, R_{ct}, and Z_W on Z are small. Second, at the electrode implantation site in a living body, reactive species (ions, proteins, and amino acids) can cause charge-transfer reactions even if the electrode potential is within the water potential window.[22–24,39] Furthermore, CIC is affected by the amount of water, ions, and dissolved oxygen around the FLiP electrode.[40] Third, the large differences between the individual FLiP electrodes are due to the fact that they were fabricated from a Pt bar by lathing and laser-irradiation porosity processing. In particular, the electrochemical properties of FLiP electrodes are significantly affected by variations in the oxidation state of their surface.[14] Given that the previously mentioned effects are included in Z, the correlation between CIC and Z was weak.

Z is useful as a rough indicator of whether the stimulation performance of the FLiP electrode is maintained during the stimulation period. Herein, the application of an excessive stimulation current of 1.5 mA for six months neither significantly affected the CIC of the implanted FLiP electrode nor caused tissue or electrode damage.[14] In addition, the equivalent circuit elements, which reflect the electrochemical properties of the FLiP electrode evaluated herein, were also stable during the six-month stimulation period (Fig. 6). Therefore, changes in the electrode characteristics should be reflected in the electrode impedance.

Commercially available active implants (or those under development) generally detect wire breakage or short-circuiting by measuring single-frequency impedance or calculating impedance from the peak load voltage and peak stimulation current.[36–38] Under normal conditions, these impedances provide mixed information on the volume resistance (ohmic drop) and polarization potential, reflecting only the device load. Therefore, these fault-detection methods are simple and effective. In contrast, EIS-ECA allows the separate observation of the response of the implanted electrode to encapsulation and electrochemical property changes at the electrode interface. Hence, the proposed method can be considered as a powerful and effective tool for the early-stage development of stimulation electrodes for active implantable devices.

5. Conclusions

The electrochemical properties of a bullet-shaped porous Pt (FLiP) electrode were evaluated during the long-term *in vivo* stimulation induced by the six-month application of an excessive stimulation current. EIS-ECA using a Randles circuit model was carried out for the performance evaluation. The results showed that the stimulation current induced the desorption of the adsorbed protein on the implanted electrodes and cleaned up their surface to facilitate ion diffusion and charge-transfer reactions. In addition to the effect of protein desorption, the change in the ion concentration due to the electrolysis of water induced an increase in C_{dl}. The generated H_2 molecules *in situ* were trapped in the pores on the FLiP electrode surface and were therefore engaged in a reversible redox reaction to induce a pseudocapacitive current.[34] The CIC improvement was caused by the contribution of the capacitive current due to C_{dl} and the pseudocapacitive current due to the redox reaction of the H_2 molecules. These are unique features of the FLiP electrode. As the electrochemical properties of the FLiP electrode were stable throughout the stimulation period, we concluded that the properties of this electrode in the chronic phase can be estimated from those in the acute phase.

EIS-ECA can clarify the complex phenomena occurring in a living body and is therefore useful for evaluating the properties and performance of implantable electrodes in the chronic phase. By comparing these results with those of other *in vitro/in vivo* experiments, we can characterize the desired specifications of the implantable stimulation electrode and provide feedback on device development at an early stage. This will facilitate the development of stimulation electrodes and avoid ethical issues by reducing animal testing. The results of this study can help in the development of more effective and safer neuroprosthetic devices in the future.

Acknowledgments

References

1 M. S. Humayun, E. De Juan, G. Dagnelie, R. J. Greenberg, R. H. Propst, and D. H. Phillips: Arch. Ophthalmol. **114** (1996) 40. https://doi.org/10.1001/archopht.1996.01100130038006
2 M. S. Humayun, J. D. Dorn, L. da Cruz, G. Dagnelie, J. A. Sahel, P. E. Stanga, A. V. Cideciyan, J. L. Duncan, D. Eliott, E. Filley, A. C. Ho, A. Santos, A. B. Safran, A. Arditi, L. V. Del Priore, and R. J. Greenberg; Argus II Study Group: Ophthalmology **119** (2012) 779. https://doi.org/10.1016/j.ophtha.2011.09.028
3 K. Stingl, K. U. Bartz-Schmidt, D. Besch, A. Braun, A. Bruckmann, F. Gekeler, U. Greppmaier, S. Hipp, G. Hörtdörfer, C. Kernstock, A. Koitschev, A. Kusnyerik, H. Sachs, A. Schatz, K. T. Stingl, T. Peters, B. Wilhelm, and E. Zrenner: Proc. Biol. Sci. **280** (2013) 20130077. https://doi.org/10.1098/rspb.2013.0077
4 A. Santos, M. S. Humayun, E. de Juan Jr, R. J. Greenburg, M. J. Marsh, I. B. Klock, and A. H. Milam: Arch. Ophthalmol. **115** (1997) 511. https://doi.org/10.1001/archopht.1997.01100150513011

5   P. M. Lewis, L. N. Ayton, R. H. Guymer, A. J. Lowery, P. J. Blamey, P. J. Allen, C. D. Luu, and J. V. Rosenfeld: ANZ J. Surg. **86** (2016) 654. https://doi.org/10.1111/ans.13616

6   A. C. Ho, M. S. Humayun, J. D. Dorn, L. da Cruz, G. Dagnelie, J. Handa, P. O. Barale, J. A. Sahel, P. E. Stanga, F. Hafezi, A. B. Safran, J. Salzmann, A. Santos, D. Birch, R. Spencer, A. V. Cideciyan, E. de Juan, J. L. Duncan, D. Eliott, A. Fawzi, L. C. Olmos de Koo, G. C. Brown, J. A. Haller, C. D. Regillo, L. V. Del Priore, A. Arditi, D. R. Geruschat, and R. J. Greenberg; Argus II Study Group: Ophthalmology. **122** (2015) 1547. https://doi.org/10.1016/j.ophtha.2015.04.032

7   H. Kanda, T. Morimoto, T. Fujikado, Y. Tano, Y. Fukuda, and H. Sawai: Invest. Ophthalmol. Vis. Sci. **45** (2004) 560. https://doi.org/10.1167/iovs.02-1268

8   K. Nakauchi, T. Fujikado, H. Kanda, T. Morimoto, J. S. Choi, Y. Ikuno, H. Sakaguchi, M. Kamei, M. Ohji, T. Yagi, S. Nishimura, H. Sawai, Y. Fukuda, and Y. Tano: Graefes. Arch. Clin. Exp. Ophthalmol. **243** (2005) 169. https://doi.org/10.1007/s00417-004-1060-2

9   T. Fujikado, T. Morimoto, H. Kanda, S. Kusaka, K. Nakauchi, M. Ozawa, K. Matsushita, H. Sakaguchi, Y. Ikuno, M. Kamei, and Y. Tano: Graefe. Arch. Clin. Exp. Ophthalmol. **245** (2007) 1411. https://doi.org/10.1007/s00417-007-0563-z

10   T. Fujikado, M. Kamei, H. Sakaguchi, H. Kanda, T. Endo, M. Hirota, T. Morimoto, K. Nishida, H. Kishima, Y. Terasawa, K. Oosawa, M. Ozawa, and K. Nishida: Invest. Ophthalmol. Vis. Sci. **57** (2016) 6147. https://doi.org/10.1167/iovs.16-20367

11   M. N. Shivdasani, N. C. Sinclair, L. N. Gillespie, M. A. Petoe, S. A. Titchener, J. B. Fallon, T. Perera, D. Pardinas-Diaz, N. M. Barnes, and P. J. Blamey: Bionic Vision Australia Consortium: Invest Ophthalmol Vis Sci. **58** (2017) 3962. https://doi.org/10.1167/iovs.16-21311

12   J. Jeong, S. H. Bae, K. S. Min, J. M. Seo, H. Chung, and S. J. Kim: IEEE Trans Biomed Eng. **62** (2015) 982. https://doi.org/10.1109/TBME.2014.2377197

13   Y. Terasawa, H. Tashiro, Y. Nakano, and J. Ohta: Sens. Mater. **30** (2018) 235. https://doi.org/10.18494/SAM.2018.1652

14   H. Tashiro, M. Kuwabara, Y. Nakano, Y. Terasawa, K. Osawa, Y. Yoshimura, H. Doi, and J. Ohta: Sens. Mater. **30** (2018) 251. https://doi.org/10.18494/SAM.2018.1723

15   S. Nomura, H. Tashiro, Y. Terasawa, Y. Nakano, M. Haruta, K. Sasagawa, H. Takehara, and J. Ohta: Electron. Commun. Jpn. **104** (2021) e12324. https://doi.org/10.1002/ecj.12324

16   S. Nomura, H. Tashiro, Y. Nakano, Y. Terasawa, H. Takehara, M. Haruta, K. Sasagawa, and J. Ohta: The 45th Annual International Conf. IEEE Engineering in Medicine and Biology Society (IEEE EMBC, 2023) 1518.

17   H. Tashiro, Y. Terasawa, M. Kuwabara, K. Osawa, T. Tokuda, J. Ohta, and T. Fujikado: Adv. Biomed. Eng. **6** (2017) 8. https://doi.org/10.14326/abe.6.8

18   The Association for Research in Vision and Ophthalmology (ARVO): https://www.arvo.org/About/policies/arvo-statement-for-the-use-of-animals-in-ophthalmic-and-vision-research/ (accessed August 2023).

19   S. F. Cogan: Annu. Rev. Biomed. Eng. **10** (2008) 275. https://doi.org/10.1146/annurev.bioeng.10.061807.160518

20   S. B. Brummer and M. J. Turner: IEEE Trans. Biomed. Eng. **24** (1977) 440. https://doi.org/10.1109/tbme.1977.326179

21   S. B. Brummer, J. McHardy, and M. J. Turner: Brain Behav Evol. **14** (1977) 10. https://doi.org/10.1159/000124611

22   J. McHardy, L. S. Robblee, J. M. Marston, and S. B. Brummer: Biomaterials **1** (1980) 129. https://doi.org/10.1016/0142-9612(80)90034-4

23   L. S. Robblee, J. McHardy, J. M. Marston, and S. B. Brummer: Biomaterials **1** (1980) 135. https://doi.org/10.1016/0142-9612(80)90035-6

24   L. S. Robblee, J. McHardy, W. F. Agnew, and L. A. Bullara: J Neurosci Methods. **9** (1983) 301. https://doi.org/10.1016/0165-0270(83)90062-6

25   A. R. Harris, P. Carter, R. Cowan, and G. G. Wallace: ChemElectroChem **8** (2021) 1078. https://doi.org/10.1002/celc.202001574

26   T L Rose, and L S Robblee: IEEE Trans Biomed Eng. **37** (1990) 1118. https://doi.org/10.1109/10.61038

27   N. Lewis, C. Lahuec, S. Renaud, E. McAdams, P. Bogonez-Franco, C. Lethias, S. Kellouche, F. Carreiras, A. Pinna, A. Histace, M. Boissiere, E. Pauthe, I. Lagroye, F. Soulier, S. Bernard, S. Binczak, B. Granado, P. Garda, M. Terosiet, A. Goguin, and O. Romain: Proc. 2015 IEEE Biomedical Circuits and Systems Conf. (IEEE BioCAS, 2015) 15651474. https://doi.org/10.1109/BioCAS. (2015) 7348399.

28   W. Franks, I. Schenker, P. Schmutz, and A. Hierlemann: IEEE Trans. Biomed. Eng. **52** (2005) 1295. https://doi.org/10.1109/tbme.2005.847523

29   C. Newbold, R. Richardson, R. Millard, P. Seligman, R. Cowan, and R. Shepherd: J. Neural Eng. **8** (2011) 036029. https://doi.org/10.1088/1741-2560/8/3/036029

30 M. S. Chae, Z. Yang, and W. Liu: Implantable Neural Prostheses 2: Microelectronics of Recording, Stimulation, and Wireless Telemetry for Neuroprosthetics –Design and Optimization (Springer, New York, 2010), p. 289. https://doi.org/10.1007/978-0-387-98120-8_9

31 T. Noda, Y Nakano, Y. Terasawa, M. Haruta, K. Sasagawa, T. Tokuda, and J. Ohta: Jpn. J. Appl. Phys. **57** (2018) 1002B3. https://doi.org/10.7567/JJAP.57.1002B3

32 D. R. Merrill, M. Bikson, and J. G. R. Jefferys: J. Neurosci. Methods **141** (2005) 171. https://doi.org/10.1016/j.jneumeth.2004.10.020

33 A. Allagui, H. Benaoum, and O. Olendski: Phys. A **582** (2021) 126252. https://doi.org/10.1016/j.physa.2021.126252

34 Y. Terasawa, H. Tashiro, Y. Nakano, K. Oosawa, and M. Ozawa: The 36th Annual International Conf. IEEE Engineering in Medicine and Biology Society (IEEE EMBC, 2014) 1402.

35 A. R. Harris, C. Newbold, D. Stathopoulos, P. Carter, R. Cowan, G. G. Wallace: Micromachines **13** (2022) 103. https://doi.org/10.3390/mi13010103

36 A. P. Sanderson, E. T. F. Rogers, C. A. Verschuur, and T. A. Newman: Front. Neurosci. **12** (2019) 1048. https://doi.org/10.3389/fnins.2018.01048

37 F. G. Zeng, S. Rebscher, W. Harrison, X. Sun, and H. Feng: IEEE Rev. Biomed. Eng. **1** (2008) 115. https://doi.org/10.1109/rbme.2008.2008250

38 Y. H. Luo, and L da Cruz: Br. Med. Bull. **109** (2014) 31. https://doi.org/10.1093/bmb/ldu002

39 D. B. Hibbert, K. Weitzner, and P. Carter: J. Electrochem. Soc. **148** (2001) E1. https://doi.org/10.1149/1.1344543

40 H. Tashiro, Y. Terasawa, K. Haraguchi, K. Osawa, T. Noda, T. Tokuda, and J. Ohta: Sens. Mater. **28** (2016) 1283. https://doi.org/10.18494/SAM.2016.1371